Journal of Fluorescence (2021) 31:1675–1682
https://doi.org/10.1007/s10895-021-02801-5

ORIGINAL ARTICLE

A New Reversible Colorimetric Chemosensor Based on Julolidine Moiety for Detecting F^-

Dongkyun Gil[1] · Boeon Suh[1] · Cheal Kim[1]

Received: 6 July 2021 / Accepted: 3 August 2021 / Published online: 13 August 2021

Abstract

We synthesized an original reversible colorimetric chemosensor **PDJ** ((E)-9-((2-(6-chloropyridazin-3-yl)hydrazono)methyl)-2,3,6,7-tetrahydro-1H,5H-pyrido[3,2,1-ij]quinolin-8-ol) for the detection of F^-. **PDJ** displayed a selective colorimetric detection to F^- with a variation of color from colorless to yellow. Limit of detection of **PDJ** for F^- was calculated as 12.1 μM. The binding mode of **PDJ** and F^- turned out to be a 1:1 ratio using Job plot. Sensing process of F^- by **PDJ** was demonstrated by ^{1}H NMR titration and DFT calculation studies that suggested hydrogen bond interactions followed by deprotonation. Moreover, the practicality of **PDJ** was demonstrated via a reversible test with TFA (trifluoroacetic acid).

Keywords Fluoride · Colorimetric chemosensor · Reversible · Calculations

Introduction

Fluoride is a trace element present in our bodies, which helps to care tooth, build dental enamel and prevent osteoporosis [1–5]. However, even at low concentration, long-term consumption causes bone fluoridation, decreased thyroid activity, bone disease, and adversely affecting the immune system [6–10]. In addition, fluoride is widely applied in industries such as pesticide production containing fluoride and production of steel, aluminum and ceramics. By this industrial spread, fluoride is increasing irreversible pollution to the environment [11–14]. Thus, monitoring and sensing fluoride are of great importance to health care and environment.

So far, fluoride detection techniques can be classified into several types, such as electrode methods, ^{19}F NMR analysis, fluorescence or colorimetric detection [15–20]. Among the various approaches, the most attractive is the colorimetric sensor that can detect fluoride via color changes visually without relying on expensive device use. In addition, colorimetric sensors have diverse advantages like low cost, easy method, quick response, and great selectivity [21–26].

Fluoride interacts with NH or OH groups through strong hydrogen bonds [27]. Therefore, a variety of colorimetric chemosensors which include NH or OH groups, have been designed to sense fluoride [28–34]. Julolidine moiety having an OH group is well known as a chromophore and great proton donor [35–40]. Pyridazine moiety acts as an electron withdrawing group and is also used in various biochemical and physicochemical applications [41]. Therefore, we predicted that the combination of the pyridazine group and the julolidine one may show deformation of energy transition via hydrogen bond interactions and unique sensing properties to fluoride.

Herein, we illustrate a novel reversible chemosensor **PDJ**, which was produced in one step by coupling 3-chloro-6-hydrazinylpyridazine with 8-hydroxyjulolidine-9-carboxaldehyde. **PDJ** could sense F^- by a color variation from colorless to yellow through the naked eye, show reversible reaction, and be reused by TFA (trifluoroacetic acid). Binding pattern and sensing mechanism of **PDJ** to F^- were presented by Job plot, ^{1}H NMR titration, ESI-mass spectral analyses and calculations.

Experiments

General Information

With a Varian spectrometer, ^{1}H and ^{13}C NMR data were afforded. Absorption and ESI-MS data were given with a Perkin Elmer spectrometer and a ACQUITY QDa, respectively.

✉ Cheal Kim
chealkim@snut.ac.kr

[1] Department of Fine Chem, SNUT (Seoul National Univ. of Sci. and Tech.), Seoul 01188, Korea

Synthesis of PDJ ((E)-9-((2-(6-chloropyridazin-3-yl)hydrazono) methyl)-2,3,6,7-tetrahydro-1H,5H-pyrido[3,2,1-ij] quinolin-8-ol)

3-Chloro-6-hydrazinylpyridazine ($0.9x10^{-3}$ mol, 0.133 g) and 8-hydroxyjulolidine-9-carboxaldehyde ($1.2x10^{-3}$ mol, 0.272 g) were dissolved in methanol (5.0 mL). The mixture was stirred for 8 h after a few drops of CH_3COOH were added. The yellowish-brown powder formed. Then, it was rinsed with CH_3OH, filtered and dried (yield: 32%). ^1H NMR: 11.32 (s, 1H), 10.77 (s, 1H), 8.08 (s, 1H), 7.60 (d, J =9.3 Hz, 1H), 7.21 (d, J =9.5 Hz, 1H), 6.71 (s, 1H), 3.15 (m, 4H), 2.60 (m, 4H), 1.85 (m, 4H). ^{13}C NMR: 157.1(1C), 153.4(1C), 146.7(1C), 146.5(1C), 144.7(1C), 129.8(1C), 127.5(1C), 115.3(1C), 112.6(1C), 106.4(2C), 49.2(1C), 48.8(1C), 26.7(1C), 21.5(1C), 20.7(1C), 20.3(1C). ESI-MS for [**PDJ** + H^+], calcd, 344.13 (m/z); found, 344.34.

UV–vis Titration

A **PDJ** stock ($5.0x10^{-3}$ M) was provided in 1,000 µL of DMSO. 12 µL of **PDJ** ($5.0x10^{-3}$ M) was diluted with 2.986 mL of CH_3CN to produce $2.0x10^{-5}$ M. TEAF (tetraethylammonium fluoride, $1x10^{-4}$ mol) was dissolved in CH_3CN (1,000 µL) and 3.0 – 33.0 µL of the F^- ($1x10^{-1}$ M) was added to $2.0x10^{-5}$ M of **PDJ**. UV-vis spectra were measured after 8 s.

Job Plot

Solutions having **PDJ** (100 µM) and TEAF (100 µM) were made. Amounts of **PDJ** and F^- kept steady (3,000 µL) and acetonitrile as solvent was employed. UV-vis spectra were measured after 8 s. Job plot was drawn by plotting against the molar fraction of fluoride under the constant total concentration (100 µM). A is the absorbance of **PDJ** after addition of F^-, and A_0 is the absorbance of the free **PDJ** at 414 nm.

Competitive Test

A **PDJ** stock ($5.0x10^{-3}$ M) was provided in 1,000 µL of DMSO. In cells containing 3,000 µL of CH_3CN, 27 µL of other anion stocks (I^-, NO_2^-, Br^-, SCN^-, OAc^-, Cl^-, $H_2PO_4^-$, N_3^-, BzO^-, CN^- and S^{2-}; 100 mM) was diluted to produce 45 equiv. 27 µL of TEAF ($1x10^{-1}$ M) was added to each cell. 12 µL ($5.0x10^{-3}$ M) of **PDJ** was added to the cell. UV-vis spectra were measured after 8 s.

^1H NMR Titration

Five NMR tubes containing **PDJ** (4.8 mg, $1.4x10^{-5}$ mol) dissolved in DMSO-d_6 (1,400 µL) were provided. Five varied equivalents (0, 0.5, 1, 2 and 5) of TEAF dissolved in DMSO-d_6 were put into five NMR tubes. ^1H NMR spectra were measured after 8 s.

Reversible UV–vis Titration

A **PDJ** stock ($5.0x10^{-3}$ M) was provided in 1,000 µL of DMSO and a F^- stock (100 mM) was provided in CH_3CN (1 mL). 12 µL of **PDJ** ($5x10^{-3}$ M) and 27 µL of F^- were diluted with 2.961 mL of CH_3CN. Then, 1.2 – 18.0 µL of TFA ($5x10^{-2}$ M) were added to a mixture of **PDJ** and F^-. UV-vis spectra were measured after 8 s.

Theoretical Studies

To apprehend geometry structures and energy transition states of **PDJ** and **PDJ** with F^-, calculations were worked through Gaussian 16 program [42]. We used B3LYP and DFT calculations for geometry optimization, and applied the 6-31G(d,p) basis set to all atoms [43–46]. Imaginary frequencies were not displayed for optimized patterns of **PDJ** and **PDJ** with F^-, indicating that the optimized geometry signified local minima. To consider the solvent interaction

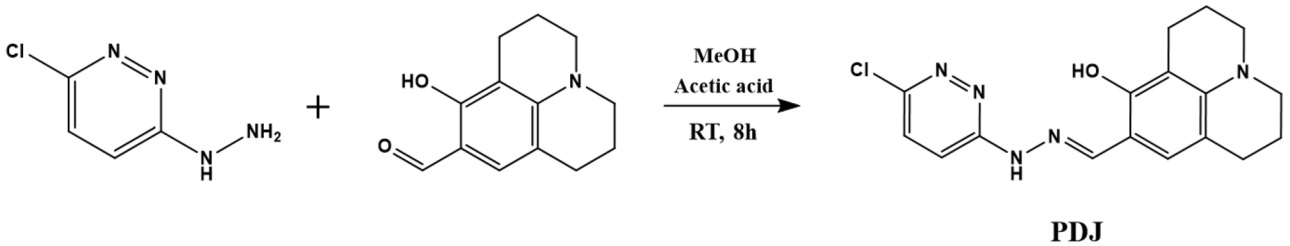

PDJ

Scheme 1 Synthetic route of PDJ

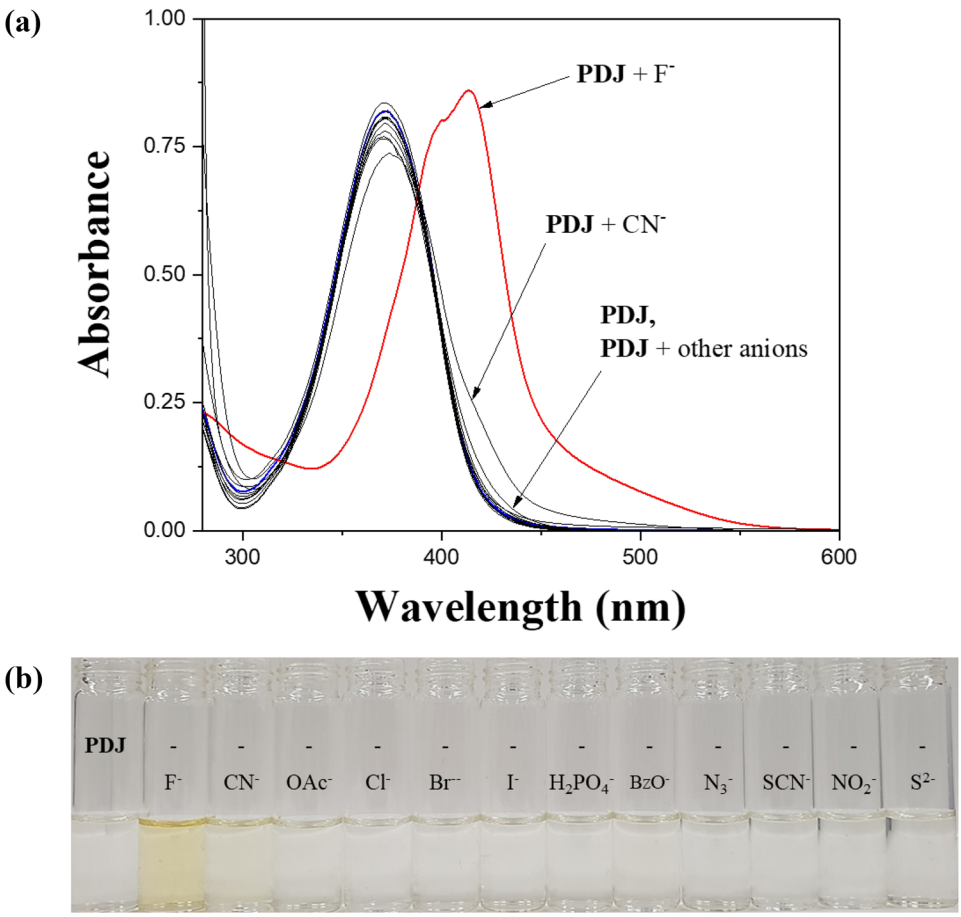

Fig. 1 (**a**) Absorbance variation of PDJ (2×10^{-5} M) with varied anions (45 equiv). (**b**) Colorimetric response of PDJ (2×10^{-5} M) upon addition of varied anions (45 equiv)

to **PDJ**, IEFPCM model was applied in all DFT calculations [47]. **PDJ** was placed into a small cavity surrounded by a dielectric continuum of given solvent CH_3CN ($\varepsilon = 35.688$). Based on the optimized patterns of **PDJ** and **PDJ** with F^-, TD-DFT calculations were performed and twenty of UV-vis transition states were investigated.

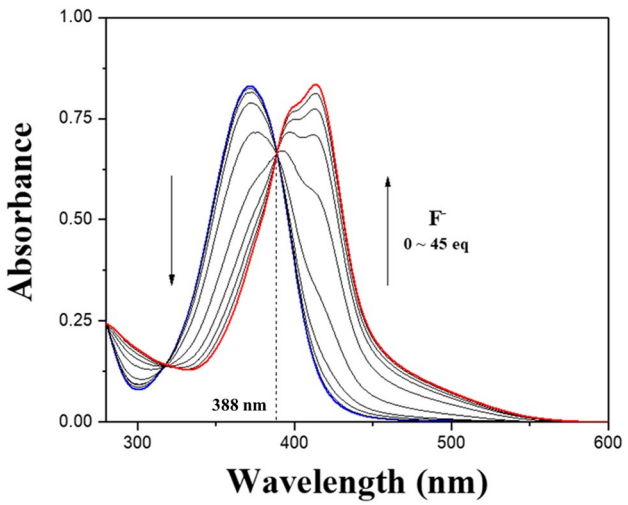

Fig. 2 Absorbance variations of PDJ (2×10^{-5} M) with increment of F^-

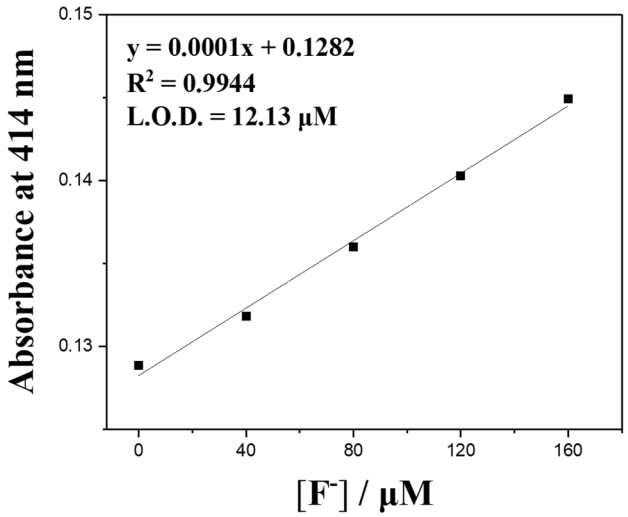

Fig. 3 Determination of the detection limit of PDJ (2×10^{-5} M) for F^- on the basis of the calibration curve

Results and Discussion

PDJ was synthesized by the coupling reaction between 3-chloro-6-hydrazinylpyridazine and 8-hydroxyjulolidine-9-carboxaldehyde (Scheme 1). **PDJ** was affirmed by ^{1}H NMR, ^{13}C NMR and ESI-MS (Figs. S1, S2 and S3).

Colorimetric Response of PDJ to F^-

Colorimetric probing capabilities of receptor **PDJ** with varied anions in CH_3CN were studied with UV-vis spectroscopy (Fig.1a). On addition of anions (45 equiv), **PDJ** exhibited little variation in absorption spectra except CN^- and F^-. The addition of CN^- to **PDJ** displayed that the absorbance at 414 nm increased slightly. However, its solution color did not change. In contrast, the addition of F^- to **PDJ** displayed that the absorbance at 414 nm remarkably increased and its solution color varied from colorless to yellow (Fig. 1b). This outcome suggested that **PDJ** can be a clearly selective colorimetric receptor for F^-.

Binding characters of **PDJ** with fluoride were investigated through UV-vis titration (Fig. 2). On the addition of F^-, the absorbance at 372 nm consistently decreased and that at 414 nm increased constantly with a saturation at 45 equiv of F^-. Complete isosbestic point emerged at 388 nm, meaning that a species was formed from the interaction of **PDJ** and F^-. The bathochromic shift drove us to presume the transition of intramolecular charge transfer (ICT) band via deprotonation of **PDJ** by F^- [48].

Job plot was executed to comprehend the binding stoichiometry of **PDJ** and F^- (Fig. S4). When the ratio ($[F^-]/([\mathbf{PDJ}]+[F^-])$) was 0.5, the value of $A\text{-}A_0$ at 424 nm was the largest, suggesting that **PDJ** reacted with F^- through a 1:1 ratio. Binding constant of **PDJ** with F^- was afforded to be $8.9\times10\ M^{-1}$ ($R^2 = 0.9914$) with Li's equation (Fig. S5) [49]. Detection limit of **PDJ** for F^- was calculated 12.1 μM using $3\sigma/K$ (Fig. 3), which is low compared to those of colorimetric F^- sensors (Table S1) [50].

A competing test was applied to extend the sensing ability of **PDJ** (Fig. 4a). S^{2-} inhibited naked-eye sensing of F^- by

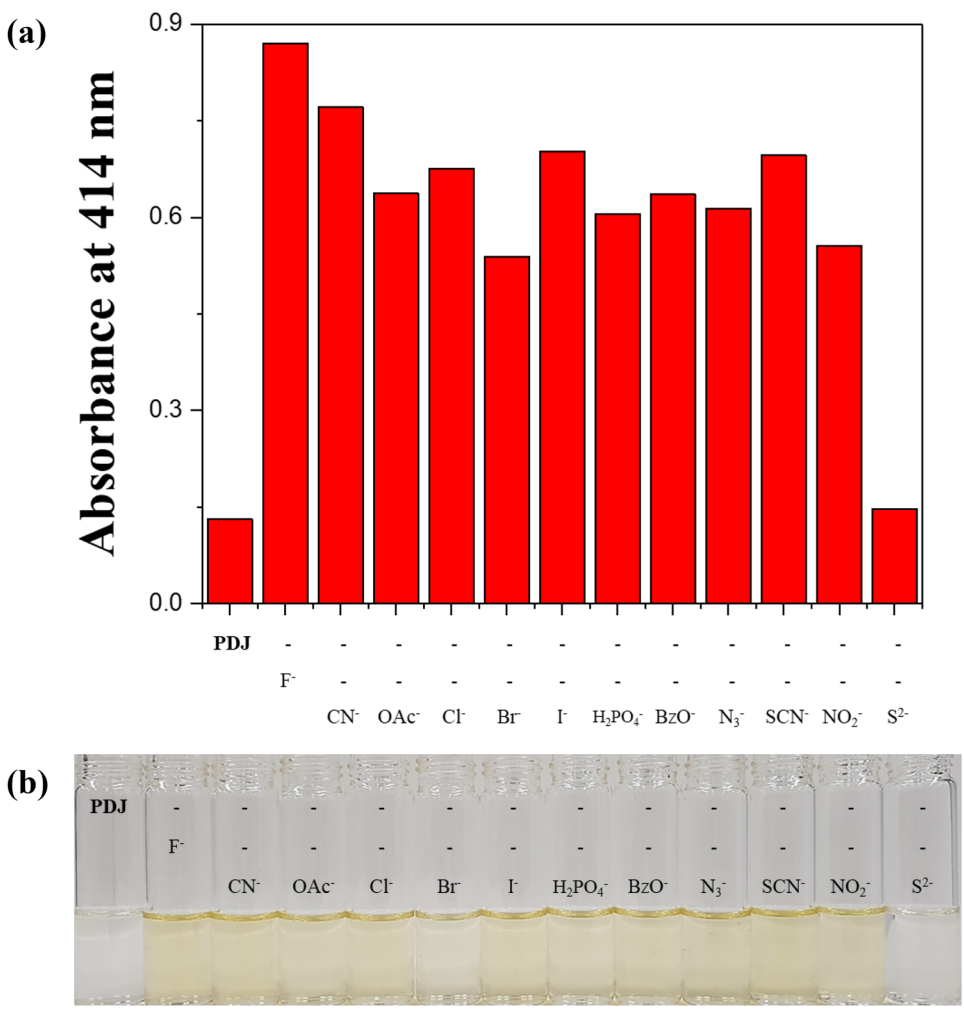

Fig. 4 (**a**) Competitive selectivity of PDJ (2×10^{-5} M) to F^- (45 equiv) with various anions (45 equiv). (**b**) Colorimetric response of PDJ (2×10^{-5} M) to F^- (45 equiv) with other anions (45 equiv)

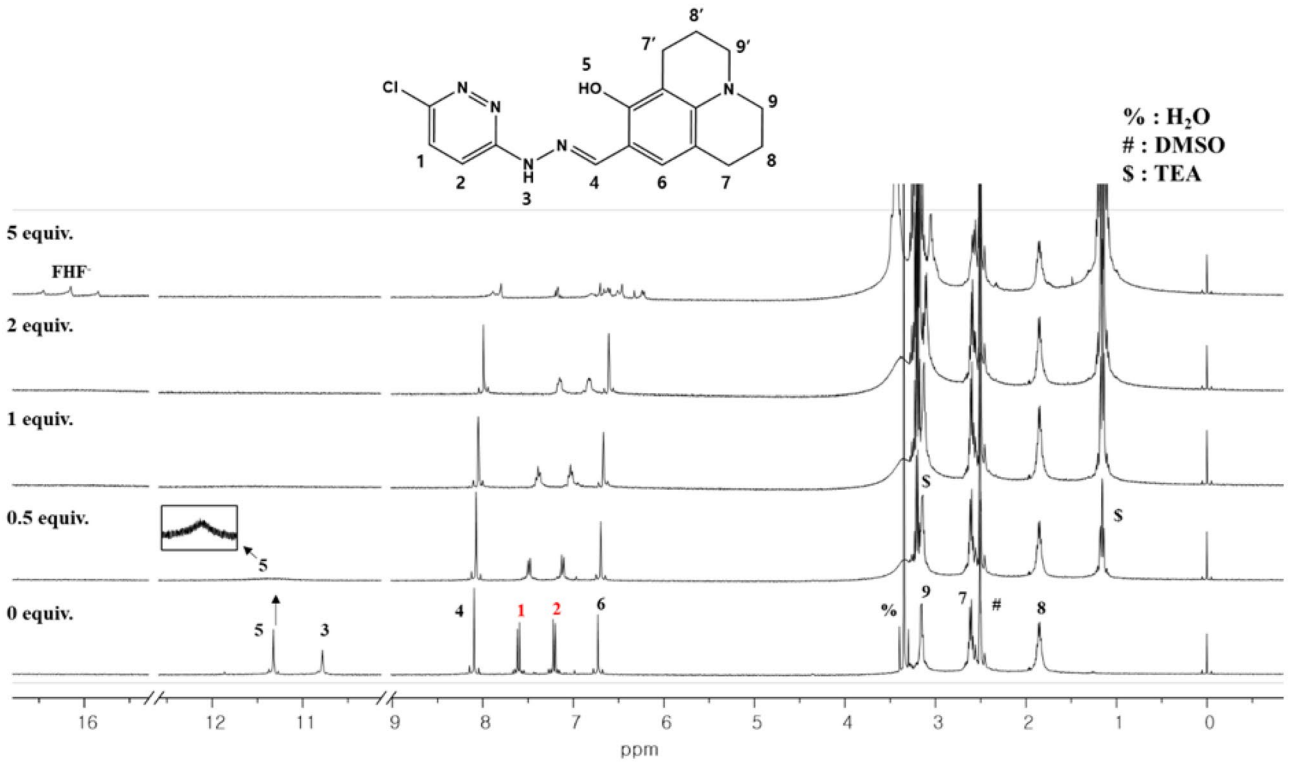

Fig. 5 ^{1}H NMR titration of PDJ with F^{-}

PDJ. The rest of the anions interfered little with absorbance (10 – 40%) at 414 nm. However, there was no problem observing color changes with the naked eye (Fig. 4b). These outcomes signified that **PDJ** may work as a clearly colorimetric sensor for fluoride with varied competing anions.

The ^{1}H NMR titration further demonstrated the reaction between **PDJ** and fluoride (Fig. 5). The OH proton (H_5) and the NH proton (H_3) of **PDJ** were displayed, respectively, as a singlet at 11.3 ppm and 10.8 ppm. With addition of half equiv of F^{-}, the H_3 disappeared and the H_5 was reduced owing to H-bonding between fluoride and H_3 and H_5. With addition of one equiv of F^{-}, the H_5 also disappeared. With excess addition of F^{-} to **PDJ**, a new triplet peak at 16.2 ppm was displayed, signifying the generation of FHF^{-} species through deprotonation of H_5 in **PDJ** by F^{-}. This presumed that the negative charge formed from the deprotonation of a hydroxyl group of **PDJ** by fluoride might be delocalized through the benzene ring and Schiff base. Deprotonation of H_5 in **PDJ** by F^{-} was further affirmed by an ESI-MS test (Fig. S6). Negative-ion data of **PDJ** with F^{-} displayed the number of 342.19 (m/z), assignable to $[\mathbf{PDJ} - H^{+}]^{-}$ (calcd; 342.11). Based on Job plot, ^{1}H NMR titrations and ESI-MS, the appropriate probing process of F^{-} by **PDJ** was suggested in Scheme 2.

To examine the reversibility of **PDJ** to F^{-}, TFA was put to the solution of **PDJ** and F^{-}. (Fig. 6). Upon addition of TFA, absorbance at 414 nm constantly decreased and that at 372 nm continually increased. The last UV-visible spectrum was same as that of **PDJ**. On addition of F^{-} again, the absorbance of 372 and 414 nm was returned. The variations of absorbance were reversible even in third cycles with the subsequently alternating addition of F^{-} and TFA (Fig. S7). These results suggested that **PDJ** can be easily recycled through treatment with appropriate reagents like TFA.

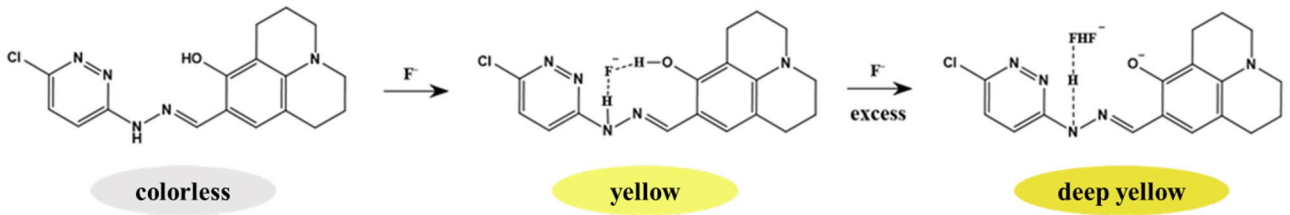

Scheme 2 Proposed probing mechanism of PDJ for F^{-}

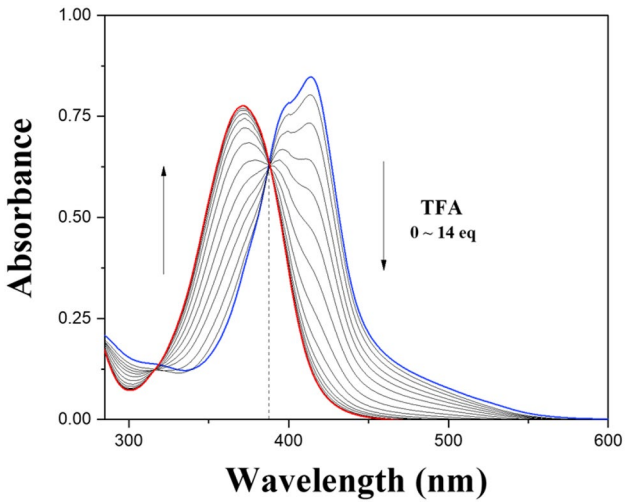

Fig. 6 Absorbance variations of PDJ (2×10^{-5} M) with increment of TFA

Theoretical Calculations

With reference to the outcomes of ESI-MS and Job plot, optimized structures of **PDJ** and **PDJ** with F^- were investigated (Fig. 7). Dihedral angle of **PDJ** was 179.632° and exhibited a planer structure (Fig. 7a). Dihedral angle of **PDJ** with F^- was –2.246° and also showed a planer structure (Fig. 7b).

Based on energy-optimized patterns of **PDJ** and **PDJ** with F^-, TD-DFT calculations were performed. For **PDJ**, the big absorption band occurred from the HOMO → LUMO+1 (372.37 nm, Fig. S8), indicating that ICT occurred from the julolidine to the pyridazine. For **PDJ** with F^-, absorption band relevance with red-shift stemmed from HOMO → LUMO+1 transition (415.96 nm, Fig. S9) and exhibited π → π* transition. In the category of the major excited states of **PDJ** and **PDJ**-F^-, their molecular orbitals and transition energies are shown in Fig. S10. With addition of F^- to **PDJ**, the decrease of HOMO to LUMO+1 energy gap would be caused by the deprotonation of –OH proton and hydrogen bonding of –NH proton, which subsequently results in bathochromic shift. In addition, the red-shift recorded in the UV-visible experiment was well consistent with the calculated results. Based on diverse spectroscopic analyses and calculations, we envisioned the plausible detection process of **PDJ** to F^- (Scheme 2).

Conclusion

We synthesized a reversible colorimetric chemosensor **PDJ** for detecting F^-. **PDJ** exhibited selectivity only to F^- by responding colorless to yellow. The limit of detection for F^- was 12.1 μM. Especially, **PDJ** can detect F^- with little interference in other anions except for S^{2-}. Moreover, **PDJ**

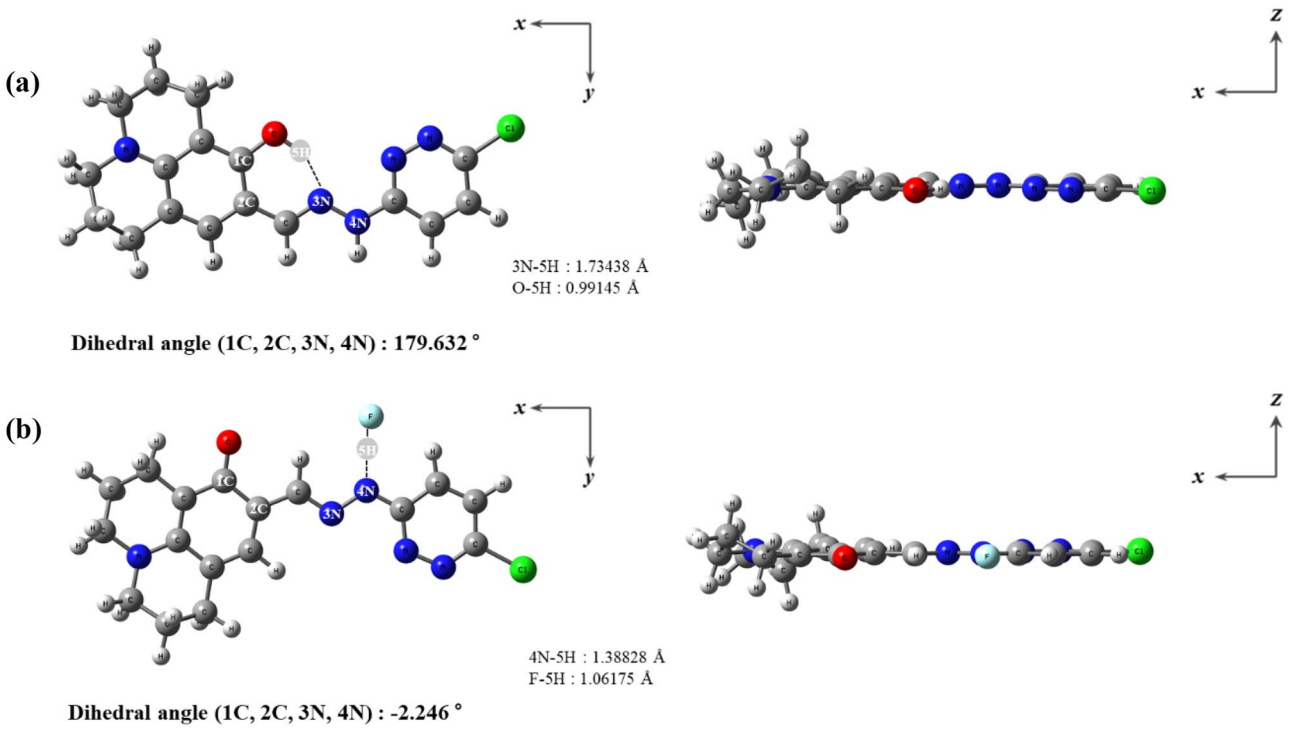

Fig. 7 Energy-optimized patterns of (**a**) PDJ and (**b**) PDJ with F^-

can be simply recycled through treatment with appropriate reagents such as TFA. The binding character and sensing process of **PDJ** with F^- were demonstrated by Job plot, ^1H NMR titration, DFT calculation and ESI-MS. We believe that a new reversible sensor **PDJ** may contribute to designing a useful fluoride probe.

Supplementary Information The online version contains supplementary material available at https://doi.org/10.1007/s10895-021-02801-5.

Acknowledgements We politely acknowledged National Research Foundation of Korea (2018R1A2B6001686).

Authors' Contributions Dongkyun Gil (60% contributions), Boeon Suh (10% contributions), Cheal Kim (30% contributions).

Declarations

Ethical Approval This article does not contain any studies with human or animal subjects.

Conflict of Interest The authors declare that they have no known competing financial interests or personal relationships that could have appeared to influence the work reported in this paper.

References

1. Sahu S, Sikdar Y, Bag R et al (2019) Visual detection of fluoride ion based on ICT mechanism. Spectrochim Acta - Part A Mol Biomol Spectrosc 213:354–360
2. Gupta N, Singhal D, Singh AK et al (2017) A highly selective chromogenic sensor for Mn2+, turn-off fluorometric for Hg2+ ion, and turn-on fluorogenic sensor for F^- ion with the practical application. Spectrochim Acta - Part A Mol Biomol Spectrosc 176:38–46
3. Singh A, Tom S, Trivedi DR (2018) Aminophenol based colorimetric chemosensor for naked-eye detection of biologically important fluoride and acetate ions in organo-aqueous medium: Effective and simple anion sensors. J Photochem Photobiol A Chem 353:507–520
4. Lim C, Seo H, Choi JH et al (2018) Highly selective fluorescent probe for switch-on Al^{3+} detection and switch-off F^- detection. J Photochem Photobiol A Chem 356:312–320
5. Zhang YM, He JX, Zhu W et al (2019) Novel pillar[5]arene-based supramolecular organic framework gel for ultrasensitive response Fe^{3+} and F^- in water. Mater Sci Eng C 100:62–69
6. Jeong HY, Lee SY, Kim C (2017) Furan and Julolidine-Based "Turn-on" Fluorescence Chemosensor for Detection of F^- in a Near-Perfect Aqueous Solution. J Fluoresc 27:1457–1466
7. Ding S, Xu A, Li M et al (2020) Theoretical study on the sensing mechanism of an ON1-OFF-ON2 type fluoride fluorescent chemosensor. Spectrochim Acta - Part A Mol Biomol Spectrosc 237:118397
8. Das A, Dighe SU, Das N et al (2019) β-carboline-based turn-on fluorescence chemosensor for quantitative detection of fluoride at PPB level. Spectrochim Acta - Part A Mol Biomol Spectrosc 220:117099
9. Peng Y, Dong YM, Dong M, Wang YW (2012) A selective, sensitive, colorimetric, and fluorescence probe for relay recognition of fluoride and Cu(II) ions with "off-On-Off" switching in ethanol-water solution. J Org Chem 77:9072–9080
10. Yadav P, Kumari M, Jain Y et al (2020) Antipyrine based Schiff's base as a reversible fluorescence turn "off-on-off" chemosensor for sequential recognition of Al^{3+} and F^- ions: A theoretical and experimental perspective. Spectrochim Acta - Part A Mol Biomol Spectrosc 227:117596
11. Wu N, Zhao LX, Jiang CY et al (2020) A naked-eye visible colorimetric and fluorescent chemosensor for rapid detection of fluoride anions: Implication for toxic fluorine-containing pesticides detection. J Mol Liq 302:112549
12. Gowri A, Veeraragavan V, Kathiresan M, Kathiravan A (2019) A pyrene based colorimetric chemosensor for CO_2 gas detection triggered by fluoride ion. Chem Phys Lett 719:67–71
13. Karuppiah K, Muniyasamy H, Sepperumal M, Ayyanar S (2020) Design and synthesis of new salicylhydrazone tagged indole derivative for fluorometric sensing of Zn^{2+} ion and colorimetric sensing of F^- ion: Applications in live cell imaging. Microchem J 159:105543
14. Landge SM, Lazare DY, Freeman C et al (2020) Rationally designed phenanthrene derivatized triazole as a dual chemosensor for fluoride and copper recognition. Spectrochim Acta - Part A Mol Biomol Spectrosc 228:117758
15. Ma L, Leng T, Wang K et al (2017) A coumarin-based fluorescent and colorimetric chemosensor for rapid detection of fluoride ion. Tetrahedron 73:1306–1310
16. Fang H, Gan Y, Wang S, Tao T (2018) A selective and colorimetric chemosensor for fluoride based on dimeric azulene boronate ester. Inorg Chem Commun 95:17–21
17. Dong M, Peng Y, Dong YM et al (2012) A selective, colorimetric, and fluorescent chemodosimeter for relay recognition of fluoride and cyanide anions based on 1,1′-binaphthyl scaffold. Org Lett 14:130–133
18. Lin Q, Gong GF, Fan YQ et al (2019) Anion induced supramolecular polymerization: A novel approach for the ultrasensitive detection and separation of F^-. Chem Commun 55:3247–3250
19. Rajasekhar K, Narayanaswamy N, Murugan NA et al (2016) A High Affinity Red Fluorescence and Colorimetric Probe for Amyloid β Aggregates. Sci Rep 6:1–10
20. Goswami S, Hazra A, Chakrabarty R, Fun HK (2009) Recognition of carboxylate anions and carboxylic acids by selenium-based new chromogenic fluorescent sensor: A remarkable fluorescence enhancement of hindered carboxylates. Org Lett 11:4350–4353
21. Lee HJ, Park SJ, Sin HJ et al (2015) A selective colorimetric chemosensor with an electron-withdrawing group for multi-analytes CN^- and F^-. New J Chem 39:3900–3907
22. Beneto AJ, Siva A (2017) A phenanthroimidazole based effective colorimetric chemosensor for copper(II) and fluoride ions. Sens Actuators B Chem 247:526–531
23. Moon KS, Singh N, Lee GW, Jang DO (2007) Colorimetric anion chemosensor based on 2-aminobenzimidazole: naked-eye detection of biologically important anions. Tetrahedron 63:9106–9111
24. Anbu Durai W, Ramu A (2020) Hydrazone Based Dual – Responsive Colorimetric and Ratiometric Chemosensor for the Detection of Cu^{2+}/F^- Ions: DNA Tracking, Practical Performance in Environmental Samples and Tooth Paste. J Fluoresc 30:275–289
25. Zabihi FS, Mohammadi A (2020) Synthesis and application of a new chemosensor based on the thiazolylazo-quinazolinone hybrid for detection of F^- and S^{2-} in aqueous solutions. Spectrochim Acta - Part A Mol Biomol Spectrosc 238:118439
26. Chatterjee C, Sethi S, Mukherjee V et al (2020) Triazole derived azo-azomethine dye as a new colorimetric anion chemosensor. Spectrochim Acta - Part A Mol Biomol Spectrosc 226:117566
27. Shyamaprosad Goswami RC (2012) An imidazole based colorimetric sensor for fluoride anion. Eur J Chem 3:455–460

28. Wang Q, Xie Y, Ding Y et al (2010) Colorimetric fluoride sensors based on deprotonation of pyrrole-hemiquinone compounds. Chem Commun 46:3669–3671
29. dos Santos CH, Uchiyama NM, Bagatin IA (2019) Selective azo dye-based colorimetric chemosensor for F^-, CH_3COO^- and PO_4^{3-}. Spectrochim Acta - Part A Mol Biomol Spectrosc 210:355–361
30. Li Z, Wang S, Xiao L et al (2018) An efficient colorimetric probe for fluoride ion based on schiff base. Inorg Chim Acta 476:7–11
31. Zang L, Wei D, Wang S, Jiang S (2012) A phenolic Schiff base for highly selective sensing of fluoride and cyanide via different channels. Tetrahedron 68:636–641
32. Wang X, Bai T, Chu T (2021) A molecular design for a turn-off NIR fluoride chemosensor. J Mol Model 27:104
33. Helal A, Thao NTT, Lee SW, Kim HS (2010) Thiazole-based chemosensor II: Synthesis and fluorescence sensing of fluoride ions based on inhibition of ESIPT. J Incl Phenom Macrocycl Chem 66:87–94
34. Lee JJ, Park GJ, Choi YW et al (2015) Detection of multiple analytes (CN^- and F^-) based on a simple pyrazine-derived chemosensor in aqueous solution: Experimental and theoretical approaches. Sens Actuators B Chem 207:123–132
35. Jo TG, Na YJ, Lee JJ et al (2015) A diaminomaleonitrile based selective colorimetric chemosensor for copper(II) and fluoride ions. New J Chem 39:2580–2587
36. Ganesan JS, Gandhi S, Radhakrishnan K et al (2019) Execution of julolidine based derivative as bifunctional chemosensor for Zn^{2+} and Cu^{2+} ions: Applications in bio-imaging and molecular logic gate. Spectrochim Acta - Part A Mol Biomol Spectrosc 219:33–43
37. Deepa A, Srinivasadesikan V, Lee SL, Padmini V (2020) Highly Selective and Sensitive Colorimetric and Fluorimetric Sensor for Cu^{2+}. J Fluoresc 30:3–10
38. Yun D, Chae JB, Kim C (2019) A novel benzophenone-based colorimetric chemosensor for detecting Cu^{2+} and F^-. J Chem Sci 131:1–10
39. Budzák Š, Jacquemin D (2018) Excited state intramolecular proton transfer in julolidine derivatives: An: ab initio study. Phys Chem Chem Phys 20:25031–25038
40. Ryu HH, Lee YJ, Kim SE et al (2016) A colorimetric F^- chemosensor with high selectivity: experimental and theoretical studies. J Incl Phenom Macrocycl Chem 86:111–119
41. Koçak R, Dastan A (2021) Synthesis of dibenzosuberenone-based novel polycyclic π-conjugated dihydropyridazines, pyridazines and pyrroles. Beilstein J Org Chem 17:719–729
42. Frisch MJ, Trucks GW, Schlegel HB, Scuseria GE, Robb MA, Cheeseman JR, Scalmani G, Barone V, Mennucci B, Petersson GA, Nakatsuji H, Caricato M, Li X, Hratchian HP, Izmaylov AF, Bloino J, Zheng G, Sonnenberg JL, Hada M, Ehara M, Toyota K, Fukuda R, Hasegawa J, Ishida M, Nakajima T, Honda Y, Kitao O, Nakai H, Vreven T, Montgomery JA Jr, Peralta JE, Ogliaro F, Bearpark M, Heyd JJ, Brothers E, Kudin KN, Staroverov VN, Kobayashi R, Normand J, Raghavachari K, Rendell A, Burant JC, Iyengar SS, Tomasi J, Cossi M, Rega N, Millam JM, Klene M, Knox JE, Cross JB, Bakken V, Adamo C, Jaramillo J, Gomperts R, Stratmann RE, Yazyev O, Austin AJ, Cammi R, Pomelli C, Ochterski JW, Martin RL, Morokuma K, Zakrzewski VG, Voth GA, Salvador P, Dannenberg JJ, Dapprich S, Daniels AD, Farkas Ö, Foresman JB, Ortiz JV, Cioslowski J, Fox DJ (2009) Gaussian 09. Gaussian Inc, Wallingford CT
43. Becke AD (1993) Density-functional thermochemistry. III. The role of exact exchange. J Chem Phys 98:5648–5652
44. Lee C, Yang W, Parr RG (1988) Development of the Colle-Salvetti correlation-energy formula into a functional of the electron density. Phys Rev B 37:785–789
45. Hariharan PC, Pople JA (1973) The influence of polarization functions on molecular orbital hydrogenation energies. Theor Chim Acta 28:213–222
46. Francl MM, Pietro WJ, Hehre WJ et al (1982) Self-consistent molecular orbital methods. XXIII. A polarization-type basis set for second-row elements. J Chem Phys 77:3654–3665
47. Klamt A, Moya C, Palomar J (2015) A Comprehensive Comparison of the IEFPCM and SS(V)PE Continuum Solvation Methods with the COSMO Approach. J Chem Theory Comput 11:4220–4225
48. Kumari N, Jha S, Bhattacharya S (2011) Colorimetric probes based on anthraimidazolediones for selective sensing of fluoride and cyanide ion via intramolecular charge transfer. J Org Chem 76:8215–8222
49. Yang R, Li K, Wang K et al (2003) Porphyrin assembly on β-cyclodextrin for selective sensing and detection of a zinc ion based on the dual emission fluorescence ratio. Anal Chem 75:612–621
50. Olivieri AC (2014) Analytical figures of merit: From univariate to multiway calibration. Chem Rev 114:5358–5378